Heliyon 9 (2023) e21122

Contents lists available at ScienceDirect

Heliyon

journal homepage: www.cell.com/heliyon

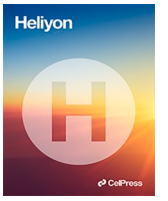

Surface enhanced Raman scattering investigation of tecovirimat on silver, gold and platinum loaded silica nanocomposites: Theoretical analysis (DFT) and molecular modeling

Nivetha G F [a], Vetrivelan V [b], Govindammal M [c], Muthu S [d], Prasath M [a,*]

[a] Department of Physics, Periyar University Centre for Post Graduate and Research Studies, Dharmapuri, 635205, India
[b] Department of Physics, Government College of Engineering, Srirangam, Tiruchirappalli, 620012, Tamilnadu, India
[c] Department of Physics, Government Arts College, Dharmapuri, 636705, India
[d] Department of Physics, Arignar Anna Govt. Arts College, Cheyyar, 604407, Tamilnadu, India

ARTICLE INFO

Keywords:
TPOXX
COVID-19
DFT
SERS
Molecular simulation
Silica nanocomposites

ABSTRACT

As of today, there have been 612 million confirmed cases of coronavirus disease (COVID-19) around the world, with over 6 million fatalities. Tecovirimat (TPOXX) is an anti-viral drug, and it was the first drug approved for the treatment of anti-pox virus in the US. However, the effectiveness of this drug against COVID-19 has not yet been explored. Since TPOXX is an anti-viral drug, an attempt has been made to determine its ability to act as a COVID inhibitor. Recent medical advances have resulted in the development of nano cage-based drug delivery. Drug delivery clusters based on nano cages have recently been used in the medical industry. As such, we used DFT coupled to the B3LYP/LANL2DZ basis set to study the adsorption behavior of the anti-viral drug TPOXX on Au/Ag/Pt···SiO_2loaded silica nanocomposites. In order to identify the active site of the molecule, we have used the frontier molecular orbital (FMO) theory of molecular electrostatic potential (MEP). The compound and its complexes obey Lipinski's rule of five and have good drug-likeness properties based on the bioactivity evaluation. The biological properties of organic molecules and nano metal clusters were compared. The TPOXX with its nanocomposites was also studied in terms of Electron Localization Function (ELF) and Localized Orbital Locator (LOL). Molecular docking was performed for both pure molecule and its silica nanocomposites-doped derivatives with the chosen proteins to discuss the protein-ligand binding properties. These results could be more helpful in designing the drug and exploring its application for the inhibition of SARS-CoV-2.

1. Introduction

SARS-CoV-2 is the genome of a single-stranded RNA-enveloped virus and is the cause of COVID-19. It was first detected in December 2019 in Wuhan, China. It is considered as a zoonotic disease, which means it is transmitted from non-human (animals) to human beings. The first case of COVID-19 transfer from human to human was identified in Guangdong, China [1]. The WHO estimates that as of April 2023, there were more than 760 million confirmed instances of infection and 6.9 million fatalities worldwide [2], which is primarily spread by contact with liquid droplets from infected people's noses when they cough or sneeze. Also, the elderly and

* Corresponding author.
E-mail address: sanprasath2006@gmail.com (P. M).

https://doi.org/10.1016/j.heliyon.2023.e21122
Received 4 August 2023; Received in revised form 16 October 2023; Accepted 16 October 2023
Available online 18 October 2023

people with underlying medical illnesses, including cancer, diabetes, chronic respiratory disease, or cardiovascular disease, are more vulnerable to this infectious disease. This predicament has motivated scientists from a variety of fields to work together to develop a vaccine for this rare sickness.

TPOXX is a drug molecule that is approved for the treatment of human small pox disease. Research into the ability of TPOXX against the pox virus had already been carried out [3,4]. The anti-viral drug TPOXX is tested against COVID-19 using DFT studies to study the exhaustive electronic properties of isolated drug delivery systems. The main objective of the present research work was to formulate, develop, and optimize TPOXX on silver, gold, and platinum-loaded silica nanocomposites (Au/Ag/Pt···SiO2) optimized using DFT in the water and gas phases. The results predicted that the complexes of TPOXX with Au/Ag/Pt···SiO_2 have enhanced biological properties than pure TPOXX. Recently, Fatmechet et al. reported Tecovirimat on a single-walled carbon nanotube [5], but no one has reported a complex of TPOXX. Because of this, we analyzed the significance of title molecule with complexes and reported the inhibition of SARS-CoV-2. TPOXX was first recognized as an anti-orthopox virus molecule in 2002 and developed by SIGA Technologies. From a result of a high-throughput screening of a chemically diverse library consisting of 350,000 unique compounds, TPOXX was identified [6,7]. TPOXX has a different mechanism of action than cidofovir, a nucleoside analog inhibiting viral DNA replication. TPOXX targets a highly conserved virally encoded protein (commonly called p37) found in all orthopox viruses without mammalian homologs [8]. During the replication cycle of orthopox virus, p37 mediates the formation of enveloped virions (EV), which is egress-competent. In vivo, mutant viruses that do not produce EVs are virulent [9–12]. It completely inhibited the CPE of the wild-type cowpox virus and extracellular vaccinia virus formation but had little effect on the intracellular formation of the vaccinia virus [13]. The in-vitro and ex-vivo permeation studies revealed that TPOXX with silica-loaded nanocomposites of silver, gold, and platinum shows a higher cumulative permeation rate compared to plain TPOXX.

In recent years, the impact of nanotechnology on the medical field has been vast. Noble metal clusters are of particular interest for their interaction and adsorption of drug molecules using DFT calculations because of the real changes in the characteristics like increased stability of drug molecules [14,15]. Different metallic nanoparticles like gold, platinum, silver, palladium, copper, zinc oxide, and metal sulphides are used in drug delivery systems [16]. N. Mahar et al. [17] studied the intermolecular interaction of gemcitabine and Au/Ag clusters, and Vetrivelan et al. [18] studied the effect of procainamide on Ag/Au-loaded silica surfaces by using the DFT-B3LYP method/LANL2DZ basis set. Silicon dioxide nanoparticles can be used as drug carriers due to their high surface area-to-volume ratio and their ability to bind to drugs [19–23]. They can improve drug solubility and bioavailability, enhance drug targeting, and reduce toxicity.

SERS is a technique for amplifying the Raman signal when molecules are adsorbed on Au or Ag-containing metal. The interaction of the adsorbed molecule with the surface of the traditional SERS substrates of Au/Ag/Cu is crucial to the performance of SERS [24,25]. In our present work, the SERS studies illustrate the adsorption and orientation of the molecules on the silicon loaded with gold, silver, and platinum (Au/Ag/Pt···SiO_2) nanocomposites. MEP analysis is used to identify the compound's charge distribution and chemical reactivity. Pharmacokinetic activity is a necessary quality of a medication candidate. The major components of the properties of drug molecules are Absorption, Distribution, Metabolism, and Excretion. The drug likeness and ADMET properties of the drug molecule are carried out to determine the drug's potential and toxicity. The initial step involved in drug discovery is identifying target biomolecules that the drug molecule binds to and inhibits.

The PLpro protein is a protease enzyme found in certain coronaviruses, including SARS-CoV-2. It is involved in viral replication and is considered a potential drug target for antiviral therapies [26]. In addition to performing the molecular docking analysis for a set of 84 chosen phytochemicals with SARS-CoV-2 main protease, Samir Chtita et al. reported that main protease (Mpro) has importance in the replication process of the virus and has been considered as a potential target in the development of novel SARS inhibitors [27–29]. Assia Belhassan et al. have already carried out molecular docking studies of various drugs with Mpro which revealed the best affinity and stability in the binding site [30,31]. The spike protein of COVID-19 is a crucial component of the SARS-CoV-2 virus, and it plays a central role in the virus's ability to infect the host cells. The spike protein specifically binds to the angiotensin-converting enzyme 2 (ACE2) receptor on the surface of human cells. This binding interaction facilitates viral entry into the host cell [32]. In this study, the antiviral efficacy of the TPOXX drug against the papain-like proteases (PLpro) of SARS-CoV-2 [PDB ID: 6WRH], COVID-19 main protease [PDB ID: 5R7Y], and SARS-CoV-2 spike receptor [PDB ID: 6M0J] will be evaluated with the aid of molecular docking calculations.

2. Computational details

The quantum chemical properties of TPOXX and its doped complexes (Ag/Au/Pt···SiO_2) were calculated using the DFT-B3LYP method and LANL2DZ basis set, which were initially developed for use in quantum mechanical calculations on transition metal complexes and demonstrated better performance for metal-ligand interactions. The molecular structure was optimized using Gaussian 09W [33], and Gauss view [34] was used to show the outcomes in the gas and water phases. The DFT method has been used to analyze the vibrational modes and the absorption between molecules and clusters using Raman and SERS intensity. Using TD-DFT and the IEFPCM solvents (DMSO, ethanol, methanol, and water), the UV–Vis was determined. MEP was used to analyze both the charge distribution of the FMO examination. Using Multiwfn software [35], the topological analysis of the ELF and LOL was performed. The theoretical technique was used to determine the thermodynamic parameters of the molecules TPOXX and TPOXX + Au/Ag/Pt···SiO_2, including entropy, enthalpy, Gibbs free energy, and specific heat capacity. The Swiss ADME [36] online server was used to analyze the chemical compounds' druglikeness and lipophilicity characteristics. The pass online tool [37], is a highest possibility online drug predictor that chooses a suitable protein to interact with the ligand. The crystal structure of COVID-19 main protease (PDB code: 5R7Y), SARS-CoV-2 spike receptor-binding domain bound with ACE 2 (PDB code: 6M0J) and papain-like protease of SARS-CoV-2 (PDB

Table 1
Optimized geometrical parameters of TPOXX and TPOXX + Ag/Au/Pt···SiO_2 at B3LYP/LANL2DZ basis set.

Parameters	TPOXX	TPOXX + SiO_2···Ag	TPOXX + SiO_2···Au	TPOXX + SiO_2···Pt
Bond length (Á)				
F(1)–C(27)	1.403	1.404	1.412	1.402
F(2)–C(27)	1.403	1.403	1.403	1.401
F(3)–C(27)	1.413	1.414	1.402	1.412
O(4)–C(18)	1.238	1.247	1.237	1.235
O(5)–C(19)	1.238	1.236	1.238	1.238
N(7)–N(8)	1.385	1.387	1.386	1.389
N(7)–C(19)	1.422	1.432	1.423	1.429
C(10)–H(29)	1.088	1.088	1.088	1.088
Bond angle (o)				
C(10)-C(9)-H(28)	119.7	119.8	119.7	119.7
N(8)-N(7)-C(18)	122.8	124.3	122.9	123.9
C(11)-C(9)-H(28)	117.9	117.9	117.9	117.8
H(30)-C(11)-H(31)	114.6	114.6	114.5	114.6
C(25)-C(23)-H(40)	119.1	119.5	119.2	119.2
C(26)-C(25)-H(42)	120.2	120.3	120.2	120.2
F(1)-C(27)-F(2)	106.8	106.7	105.7	107
C(23)-C(25)-C(26)	119.6	119.3	119.6	119.6

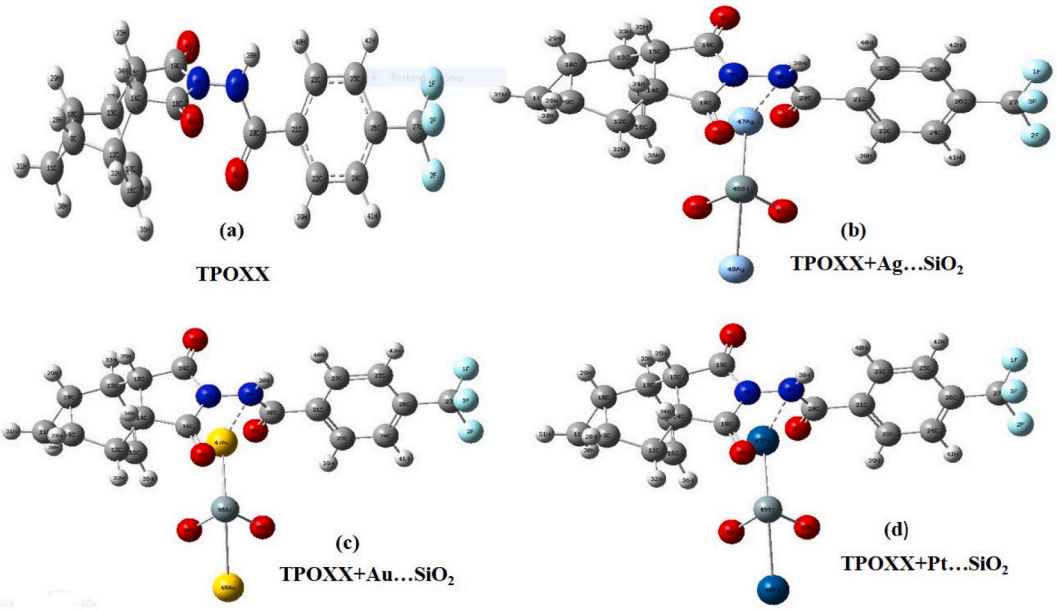

Fig. 1. Optimized structure of (a) TPOXX (b) TPOXX + Ag···SiO_2 (c) TPOXX + Au···SiO_2 (d) TPOXX + Pt···SiO_2.

code: 6WRH) was obtained from protein data bank. The ions and water from the ligand molecules were removed, and the protein was separated for the docking study. The protein (5R7Y, 6M0J, 6WRH) [38] and ligand (TPOXX and TPOXX + Au/Ag/Pt···SiO_2) interaction energy profiles were created utilizing the molecular docking experiments, which were carried out with the aid of iGEMDOCK [39,40] and visualized by using PyMOL software [41].

3. Results and discussion

3.1. Optimized geometrical parameters analysis

The geometrical parameters of the TPOXX and the complexes (TPOXX + Ag/Au/Pt···SiO_2) were calculated and tabulated in Table 1 and their optimized structure is shown in Fig. 1. Based on the B3LYP/LANL2DZ basis set, the DFT method was used to calculate the geometrical parameters of the molecules. The optimized structure of the TPOXX molecule shows various kinds of bonds: they are F–C (3), O–C (3), N–N (1), N–C (3), N–H (1), C–C (21), and C–H (14). The largest bond lengths found in TPOXX complexes are C12–C14, C9–C12, F 3-C27 and C22–C24 in the range of 1.582 Å – 1.401 Å. The theoretical lowest bond length is observed at N8–H38 [TPOXX: 1.013 Å, TPOXX + Ag···SiO_2: 1.014 Å, TPOXX + Au···SiO_2: 1.014 Å, and TPOXX + Pt···SiO_2: 1.015 Å]. After the adsorption of Ag/Au/

Table 2
Absorption energy of TPOXX and TPOXX + Ag/Au/Pt···SiO_2 obtained by B3LYP/LANL2DZ basis set.

Compound	Energy (Kcal/Mol)	Adsorption energy (Kcal/Mol)	Bond length (Å)	
TPOXX	197.71			
Ag···SiO2	5.94			
Au···SiO2	5.69			
Pt···SiO2	5.36			
TPOXX + Ag … sio2	203.72	−0.08	N(8)–Ag(47)	3.747
TPOXX + Au … sio2	203.81	−0.41	N(8)–Au(47)	4.739
TPOXX + Pt … sio2	204.7	−1.63	N(8)–Pt(47)	3.616

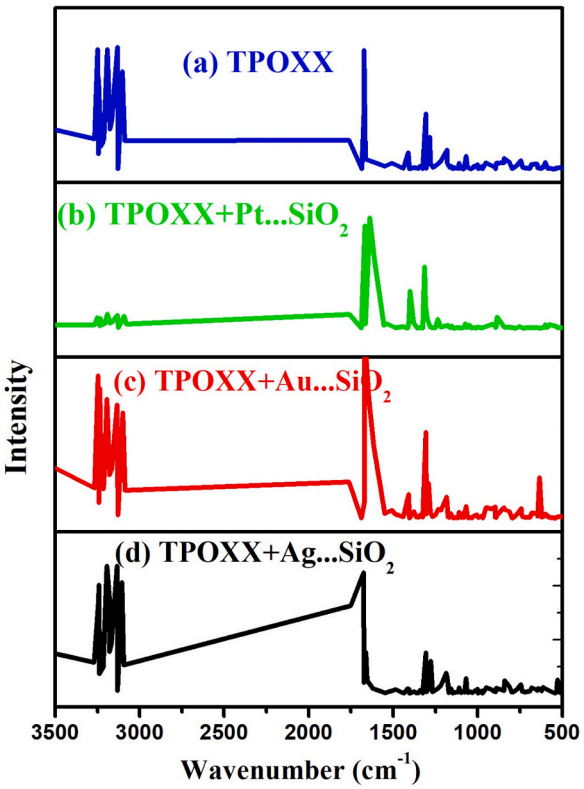

Fig. 2. Calculated Raman for (a) TPOXX and SERS spectra of (b) TPOXX + Pt···SiO_2 (c) TPOXX + Au···SiO_2 (d) TPOXX + Ag···SiO_2.

Table 3
Selected theoretical vibrational frequencies of Raman and SERS spectral parameters of TPOXX and TPOXX + Ag/Au/Pt···SiO_2 obtained by B3LYP/LANL2DZ basis set.

S. No.	Calculated Raman (TPOXX)		Calculated SERS						Assignments (PED)
			TPOXX + Ag···SiO_2		TPOXX + Au···SiO_2		TPOXX + Pt···SiO_2		
	Wavenumber (cm^{-1})	Intensity	Wavenumber (cm^{-1})	Intensity	Wavenumber (cm^{-1})	Intensity	Wavenumber (cm^{-1})	Intensity	
1	3651	168	3643	169	3641	233	3623	111	NH – Stretching
2	3248	445	3242	403	3246	531	3252	361	CH – Stretching
3	3192	445	3194	474	3193	444	3192	486	CH – Stretching
4	3090	106	3093	107	3087	104	3093	414	CH – Stretching
5	1671	442	1675	450	1669	694	1667	3521	CC – Stretching
6	1412	61	1413	19	1487	15	1401	1267	CC – Stretching
7	1284	120	1277	121	1292	131	1236	305	CC – Stretching
8	744	32	736	8	735	6	753	61	HCCC - Torsion
9	690	3	690	9	690	4	692	10	HCC – Bending
10	538	4	544	1	539	1	530	48	HCCC - Torsion

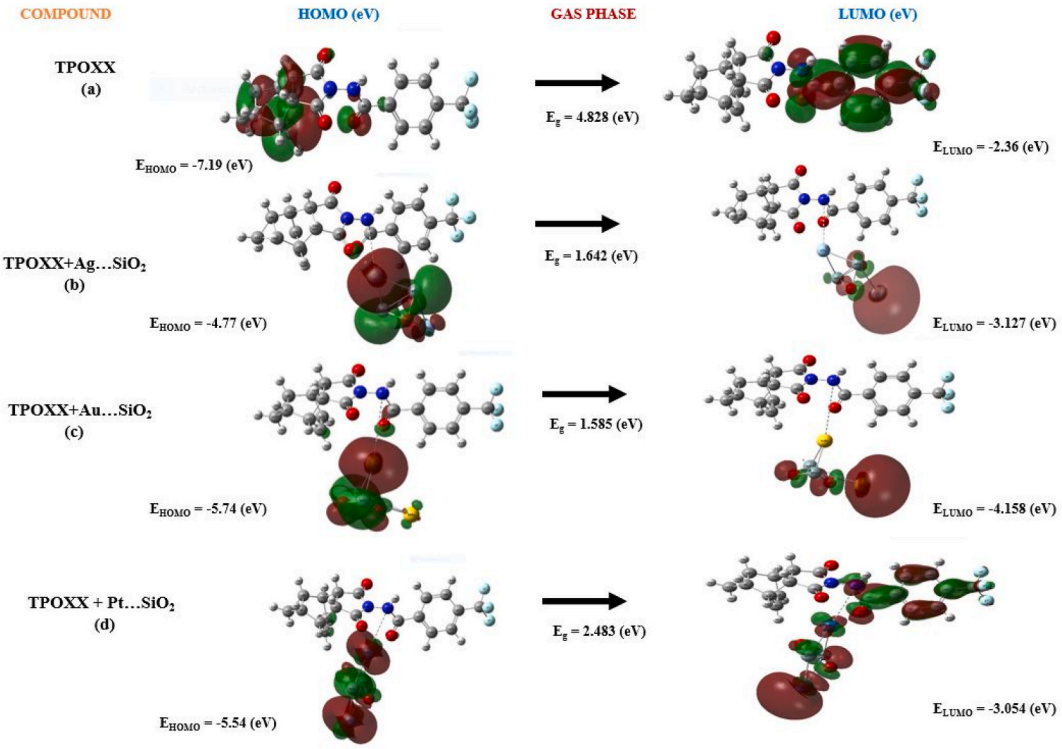

Fig. 3. HOMO – LUMO plots of (a) TPOXX, (b) TPOXX + Ag···SiO_2, (c) TPOXX + Au···SiO_2, (d) TPOXX + Pt···SiO_2 at gas phase.

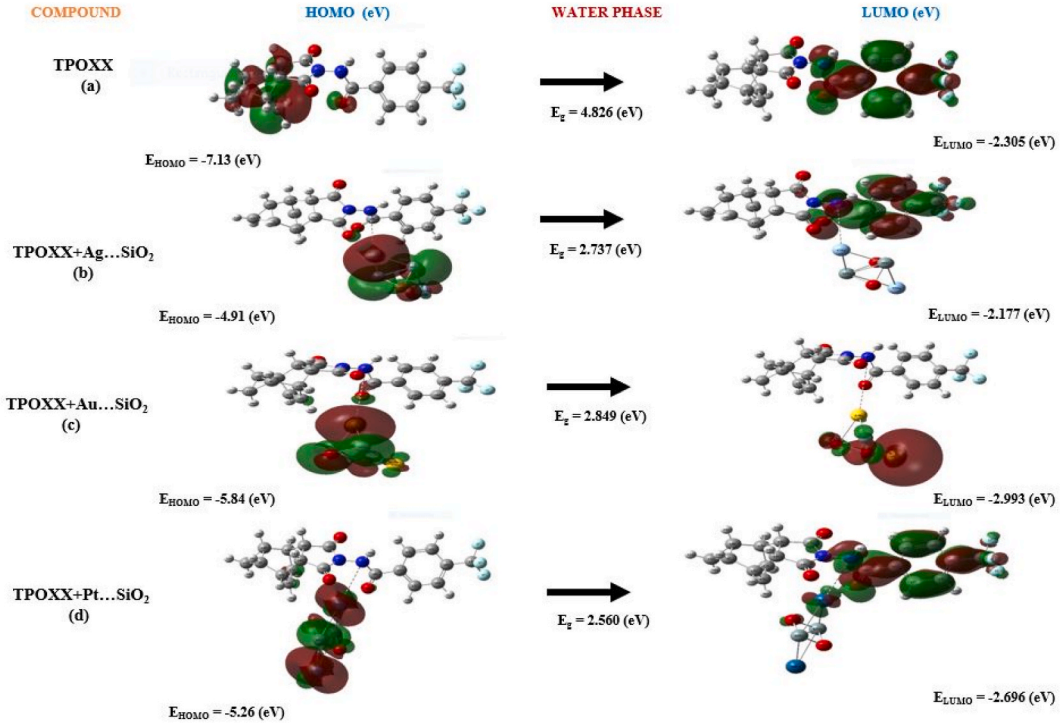

Fig. 4. HOMO – LUMO plots of (a) TPOXX, (b) TPOXX + Ag···SiO_2, (c) TPOXX + Au···SiO_2, (d) TPOXX + Pt···SiO_2 at water phase.

Table 4
Calculated chemical and electrochemical properties of TPOXX and TPOXX + Ag/Au/Pt···SiO_2 at gas and water phase using B3LYP/LANL2DZ basis set.

Parameters (eV)	TPOXX		TPOXX + Ag···SiO_2		TPOXX + Au···SiO_2		TPOXX + Pt···SiO_2	
	Gas	Water	Gas	Water	Gas	Water	Gas	Water
HOMO (E_{HOMO})	−7.19	−7.13	−4.77	−4.91	−5.74	−5.84	−5.54	−5.26
LUMO (E_{LUMO})	−2.36	−2.305	−3.127	−2.177	−4.158	−2.993	−3.054	−2.696
Energy gap (E_g)	4.828	4.826	1.642	2.737	1.585	2.849	2.483	2.56
Hardness (η)	2.414	2.413	0.821	1.368	0.792	1.425	1.242	1.28
Softness (S)	0.414	0.414	1.218	0.731	1.262	0.702	0.805	0.781
Chemical potential (μ)	−4.774	−4.718	−3.947	−3.545	−4.950	−4.417	−4.295	−3.975
Electronegativity (χ)	4.774	4.718	3.947	3.545	4.950	4.417	4.295	3.975
Electrophilicity index (ω)	4.828	4.613	9.492	4.593	15.465	6.849	7.431	6.175
Fermi level f(E)	−4.774	−4.718	−3.947	−3.545	−4.950	−4.417	−4.295	−3.975

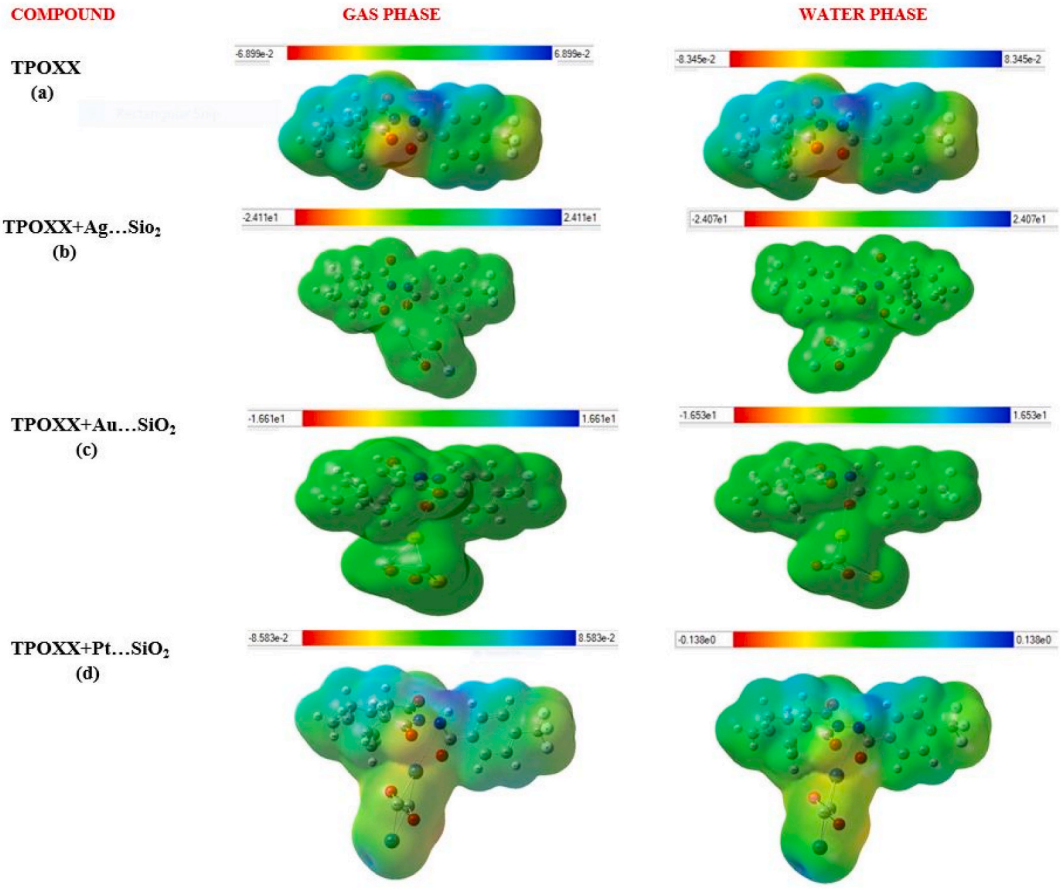

Fig. 5. MEP plots of (a) TPOXX, (b) TPOXX + Ag···SiO_2, (c) TPOXX + Au···SiO_2, (d) TPOXX + Pt···SiO_2 at gas and water phase.

Pt···SiO_2 on the TPOXX molecule, there was a slight change in the bond length and bond angle. In addition, TPOXX + Ag/Au/Pt···SiO_2 nano composites displayed no changes in the structural parameters.

3.2. Adsorption energy analysis

The organic molecule TPOXX binds with the noble metals of gold (Au), silver (Ag), and platinum (Pt) loaded silica nanocomposites (Au/Ag/Pt···SiO_2) with adsorption energies of −0.08, −0.41, and −1.63 kcal/mol, respectively. The bond length between the noble metals and the nitrogen (N) atom of TPOXX is listed in Table 2. From the observation, the highest negative value is found in the complex of TPOXX + Pt···SiO_2 with an adsorption energy of −1.63 kcal/mol, and it shows chemisorption. Due to the adsorption of the TPOXX molecule on Au/Ag/Pt···SiO_2, there is an explicit change in the FMO energy levels. There is an increase in conductivity after

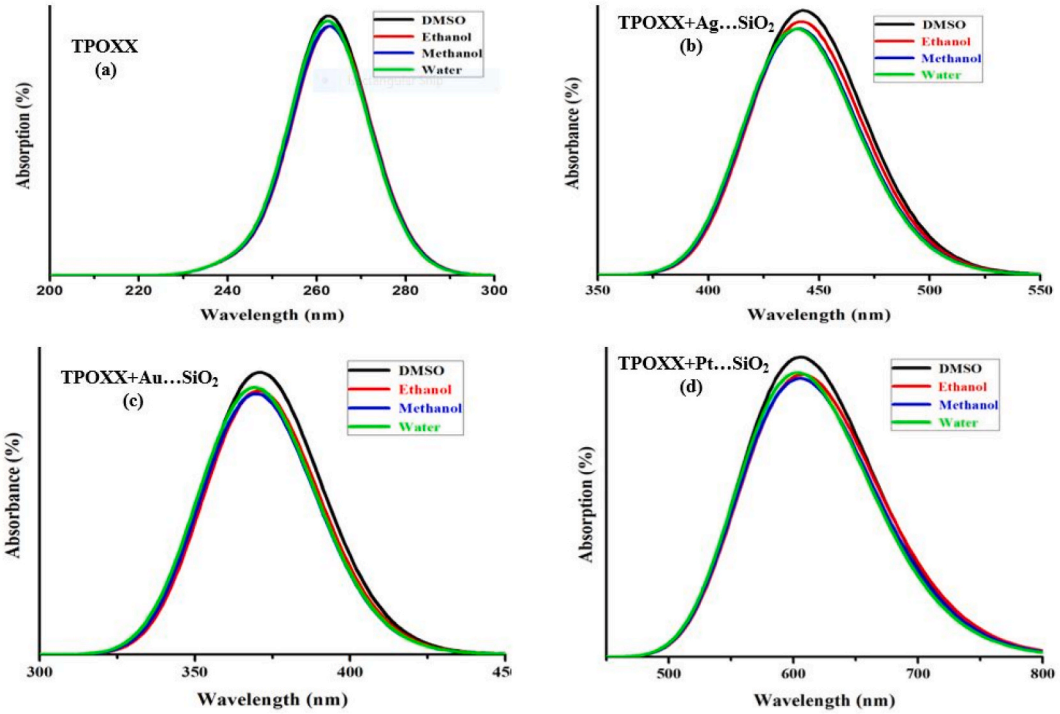

Fig. 6. UV–Vis spectra for (a) TPOXX, (b) TPOXX + Ag···SiO_2, (c) TPOXX + Au···SiO_2, (d) TPOXX + Pt···SiO_2 using different solvents (DMSO, Ethanol, Methanol, Water).

adsorption of TPOXX + Au/Ag/Pt···SiO_2 complexes, which is useful for drug delivery systems since band gap energy values gradually decrease.

3.3. SERS

It is a highly sensitive analytical technique used for the detection and characterization of molecules. In SERS, a sample is brought into contact with a metallic surface that has been roughened or coated with nanoparticles. Several orders of magnitude are added to the Raman scattering signal by the metal surface. TPOXX and TPOXX + Au/Ag/Pt···SiO_2 molecules are shown in Fig. 2 with their Raman and SERS spectra, and also their vibrational frequencies were compared and presented in Table 3. The Raman spectral line at 3651 cm^{-1} assigned to N–H stretching is shifted to 3643, 3641, and 3623 cm^{-1} for the SERS spectrum of TPOXX + Ag/Au/Pt···SiO_2 with an enhancement factor of 0.39 for Au loaded and 0.34 for Pt loaded. The normal Raman spectral line observed at 1412 cm^{-1} is shifted to 1413 cm^{-1}, 1487 cm^{-1}, and 1401 cm^{-1}, for Ag/Au/Pt...SiO_2 complexes assigned to CC stretching. The maximum enhancement factor for silver loaded nanocomposites is 0.69, 0.75, and 0.81, 0.19 for gold loaded silica nanocomposites; and 6.35, 19.77, and 11 for platinum loaded silica nanocomposites. As a result of TPOXX interaction with Ag/Au/Pt···SiO_2, various modes exhibit a blue or red shift [42].

3.4. Molecular reactivity analysis

In a molecule, the FMOs are the LUMO and HOMO, and they are responsible for many chemical properties and reactions that are calculated in both the gas and water phases, as shown in Figs. 3 and 4. After the adsorption of the TPOXX molecule with Au/Ag/Pt···SiO_2, the energy gap values show a decreasing nature Table 4. The energy gap value for the TPOXX is 4.828 eV in the gas phase and 4.826 eV in the water phase. The energy gap values of TPOXX + Ag/Au/Pt···SiO_2 were (1.642 eV, 2.737 eV), (1.585 eV, 2.849 eV), and (2.483 eV, 2.56 eV). Between the title molecule and TPOXX + Ag/Au/Pt···SiO_2, the electrophilicity increases dramatically, with the highest value found at gold (Au) loaded SiO_2 (15.465 eV) in the gas phase and the lowest value found at silver (Ag) loaded SiO_2 (4.593 eV) in the water phase. The softness of the complexes increases and the hardness of the complexes decreases when compared to the title molecule, which indicates that the complexes are more reactive [43,44].

MEP is a computational method to investigate the distribution of electrons, electrostatic properties, and binding sites of molecules, as shown in Fig. 5. The red and yellow-colored regions indicate the negative potential surface, which is responsible for the electrophilic attack. Nucleophilic attacks are caused by the positive potential surface, which is blue, and it is increasing in order from red to orange to yellow to green to blue [45].

Table 5
Prediction of wavelength, energy, oscillator strength and major contribution of TPOXX and TPOXX + Ag/Au/Pt···SiO_2 calculated at B3LYP/LANL2DZ basis set using different solvents (DMSO, ethanol, methanol and water).

Compound	Solvent	Wavelength	Bandgap (eV)	Energy	Oscillator strength	Symmetry	Major contribution
TPOXX	DMSO	263	4.71	38055	0.0022	Singlet-A	H-5- > L+1 (24 %), H-2- > L+1 (35 %)
		262	4.73	38117	0.0077	Singlet-A	H-9- > LUMO (15 %), H-7- > LUMO (17 %), H-6- > LUMO (22 %)
		243	5.10	41085	0.0006	Singlet-A	H-9- > L+1 (17 %), H-7- > L+1 (33 %), H-5- > L+4 (10 %), H-2- > L+4 (13 %)
	Ethanol	263	4.71	38028	0.0018	Singlet-A	H-5- > L+1 (22 %), H-2- > L+1 (33 %)
		263	4.71	38058	0.0077	Singlet-A	H-9- > LUMO (13 %), H-7- > LUMO (16 %), H-6- > LUMO (20 %)
		244	5.08	41054	0.0006	Singlet-A	H-9- > L+1 (18 %), H-7- > L+1 (33 %), H-5- > L+4 (10 %), H-2- > L+4 (14 %)
	Methanol	263	4.71	38045	0.002	Singlet-A	H-5- > L+1 (23 %), H-2- > L+1 (35 %)
		263	4.71	38091	0.0075	Singlet-A	H-9- > LUMO (14 %), H-7- > LUMO (17 %), H-6- > LUMO (21 %)
		243	5.10	41071	0.0006	Singlet-A	H-9- > L+1 (17 %), H-7- > L+1 (33 %), H-5- > L+4 (10 %), H-2- > L+4 (14 %)
	water	263	4.71	38071	0.0023	Singlet-A	H-5- > L+1 (24 %), H-2- > L+1 (35 %)
		262	4.73	38151	0.0074	Singlet-A	H-9- > LUMO (15 %), H-7- > LUMO (18 %), H-6- > LUMO (22 %)
		243	5.10	41101	0.0006	Singlet-A	H-9- > L+1 (17 %), H-7- > L+1 (34 %), H-5- > L+4 (10 %), H-2- > L+4 (13 %)
TPOXX + Ag···SiO_2	DMSO	449	2.76	22251	0.0687	Singlet-A	HOMO- > LUMO (53 %), HOMO- > L+1 (24 %), HOMO- > L+4 (15 %)
		438	2.83	22831	0.0805	Singlet-A	HOMO- > L+1 (37 %), HOMO- > L+3 (22 %), HOMO- > L+4 (22 %)
		425	2.92	23552	0.0065	Singlet-A	HOMO- > L+2 (95 %)
	Ethanol	449	2.76	22276	0.0617	Singlet-A	HOMO- > LUMO (56 %), HOMO- > L+1 (21 %), HOMO- > L+4 (14 %)
		437	2.84	22874	0.0781	Singlet-A	HOMO- > L+1 (39 %), HOMO- > L+3 (23 %), HOMO- > L+4 (19 %)
		432	2.87	23164	0.0087	Singlet-A	HOMO- > L+2 (92 %)
	Methanol	448	2.77	22311	0.0536	Singlet-A	HOMO- > LUMO (57 %), HOMO- > L+1 (19 %), HOMO- > L+4 (16 %)
		436	2.84	22920	0.0838	Singlet-A	HOMO- > L+1 (41 %), HOMO- > L+3 (24 %), HOMO- > L+4 (19 %)
		428	2.90	23348	0.0071	Singlet-A	HOMO- > L+2 (94 %)
	water	448	2.77	22323	0.0502	Singlet-A	HOMO- > LUMO (57 %), HOMO- > L+1 (18 %), HOMO- > L+4 (18 %)
		436	2.84	22931	0.0888	Singlet-A	HOMO- > L+1 (42 %), HOMO- > L+3 (24 %), HOMO- > L+4 (20 %)
		421	2.94	23763	0.0061	Singlet-A	HOMO- > L+2 (95 %)
TPOXX + Au···SiO_2	DMSO	435	2.85	23006	0.0003	Singlet-A	HOMO- > LUMO (72 %)
		375	3.31	26675	0.12	Singlet-A	HOMO- > L+1 (17 %), HOMO- > L+2 (66 %)
		361	3.43	27702	0.0586	Singlet-A	H-2- > LUMO (64 %)
	Ethanol	441	2.81	22696	0.0003	Singlet-A	HOMO- > LUMO (78 %)
		374	3.32	26719	0.1068	Singlet-A	H-1- > LUMO (11 %), HOMO- > L+1 (17 %), HOMO- > L+2 (63 %)
		362	3.42	27598	0.0573	Singlet-A	H-2- > LUMO (69 %)
	Methanol	437	2.84	22868	0.0003	Singlet-A	HOMO- > LUMO (76 %)
		373	3.32	26775	0.107	Singlet-A	HOMO- > L+1 (17 %), HOMO- > L+2 (63 %)
		361	3.43	27700	0.0562	Singlet-A	H-2- > LUMO (67 %)
	water	431	2.88	23177	0.0003	Singlet-A	HOMO- > LUMO (67 %), HOMO- > L+1 (14 %)
		373	3.32	26792	0.1135	Singlet-A	HOMO- > L+1 (16 %), HOMO- > L+2 (65 %)
		359	3.45	27838	0.0559	Singlet-A	H-2- > LUMO (59 %), H-2- > L+1 (14 %)
TPOXX + Pt···SiO_2	DMSO	638	1.94	15672	0.0033	Singlet-A	H-2- > L+1 (21 %), H-2- > L+5 (18 %), HOMO- > L+1 (12 %)
		619	2.00	16163	0.002	Singlet-A	H-3- > L+1 (29 %), H-3- > L+2 (10 %), H-3- > L+5 (26 %)
		586	2.12	17066	0.0058	Singlet-A	H-6- > L+1 (23 %), H-6- > L+5 (16 %), HOMO- > L+1 (16 %)
	Ethanol	641	1.93	15602	0.0033	Singlet-A	H-2- > L+1 (21 %), H-2- > L+5 (16 %), HOMO- > L+1 (12 %)
		620	2.00	16135	0.0019	Singlet-A	H-3- > L+1 (30 %), H-3- > L+2 (12 %), H-3- > L+5 (23 %)
		586	2.12	17072	0.0054	Singlet-A	H-6- > L+1 (24 %), H-6- > L+5 (14 %), HOMO- > L+1 (15 %)

(*continued on next page*)

Table 5 (*continued*)

Compound	Solvent	Wavelength	Bandgap (eV)	Energy	Oscillator strength	Symmetry	Major contribution
	Methanol	638	1.94	15666	0.0032	Singlet-A	H-2- > L+1 (21 %), H-2- > L+5 (17 %), HOMO- > L+1 (12 %)
		617	2.01	16203	0.0019	Singlet-A	H-3- > L+1 (29 %), H-3- > L+2 (11 %), H-3- > L+5 (24 %)
		584	2.12	17112	0.0053	Singlet-A	H-6- > L+1 (24 %), H-6- > L+5 (15 %), HOMO- > L+1 (15 %)
	water	635	1.95	15752	0.0032	Singlet-A	H-2- > L+1 (20 %), H-2- > L+5 (18 %), HOMO- > L+1 (12 %)
		615	2.02	16268	0.0019	Singlet-A	H-3- > L+1 (28 %), H-3- > L+5 (27 %)
		584	2.12	17134	0.0054	Singlet-A	H-6- > L+1 (23 %), H-6- > L+5 (17 %), HOMO- > L+1 (15 %)

3.5. UV–Vis. spectrum analysis

By TD-DFT, the theoretical UV–Vis. spectral properties (absorption wavelength, oscillator strength, and energy) of TPOXX and TPOXX + Ag/Au/Pt···SiO_2 were investigated in DMSO (a polar aprotic solvent), ethanol, methanol, and water (polar protic solvents).

In Fig. 6 and Table 5, the comparison spectra of the title molecule and the complexes were discussed. For the TPOXX molecule, the highest UV absorption band is found at 263 nm, whereas the complex molecules (TPOXX + Ag/Au/Pt···SiO_2) show the highest absorption peak at 449 nm, 441 nm, and 641 nm, respectively. From Tables 5 and it has been observed that the TPOXX molecule with Ag/Au/Pt···SiO_2 molecules shows a red shift in UV absorption, with the highest shift found at platinum (Pt)-loaded silica nanocomposites. The λ_{max} of different solvents was calculated, and the band gap decreases with time. Upon the interaction of nanomaterials, a band change is observed (electronically and electromagnetically) as a result of charge transfer.

3.6. Mulliken atomic charges analysis

Table 6 summarizes the Mulliken charges for TPOXX and TPOXX + Ag/Au/Pt …. SiO_2 complexes calculated using the B3LYP/LANL2DZ basis set. The TPOXX molecule is adsorbed on the silver-loaded silica nanocomposites in TPOXX + Ag...SiO_2, with N8 having the highest electronegative value (−0.3764 e) in the gas phase and (−0.3824 e) in the water phase. Due to the adsorption of TPOXX on Ag···SiO_2, the charge of N8 changes to −0.3782 e (gas phase) and −0.3786 e (water phase). In TPOXX + Au···SiO_2, the TPOXX molecule is adsorbed on the gold-loaded silica nanocomposites with the same N8 atom, and the charge changes to −0.3646 e (gas phase) and −0.3690 e (water phase). In TPOXX + Pt···SiO_2, the TPOXX molecule is adsorbed on the platinum-loaded silica nanocomposites with the N8 atom, and its charge changes to −0.3507 e (gas phase) and −0.3555 e (water phase). All the fluorine, oxygen, and nitrogen atoms of the TPOXX molecule show a negative charge, and its charge shows small variation because of the adsorption of TPOXX on the Ag/Au/Pt-loaded silica nanocomposites. All the hydrogen atoms of the TPOXX and complexes shows a positive charge.

3.7. Thermodynamic analysis

In Table 7, Gibbs free energy, entropy, and enthalpy of the molecules were calculated using the above-mentioned theoretical method in order to determine their thermal stability. The negative value of the enthalpy ($\Delta H < 0$) indicates that the reaction is exothermic. If $\Delta H > 0$, the reaction is said to be an endothermic reaction [46]. The negative value of Gibbs free energy ($\Delta G < 0$) represents the spontaneous adsorption of the TPOXX molecule on the metal-loaded silica nanocomposites. As shown in Table 7, the negative values of ΔH and ΔG suggest exothermic reactions, spontaneous interactions, and thermodynamically ordered interactions between molecules and their complexes.

3.8. ELF and LOL analysis

Using the Multiwfn program, the electron pair density of ELF and LOL are determined. Figs. 7 and 8 represent the color-shaded map of ELF and its corresponding contour maps of TPOXX and the complexes (TPOXX + Ag/Au/Pt···SiO_2). Figs. 9 and 10 represent the color-shaded map of LOL and its corresponding contour maps of TPOXX and the complexes (TPOXX + Ag/Au/Pt···SiO_2). In Fig. 7, the highest value of ELF (approximately 1) decreases from red > yellow > green > sky blue > royal blue. For the TPOXX molecule, the ELF color code is within the range of −15.67 to 15.67 $Bohr^3$. For the complexes, the ELF color code ranges from −9.89 to 19.78 $Bohr^3$ (TPOXX + Ag···SiO_2), −18.60 to 9.30 $Bohr^3$ (TPOXX + Au···SiO_2), and −9.63 to 19.25 $Bohr^3$ (TPOXX + Pt···SiO_2). The red color in the ELF graph represents the localization area of electrons, and the blue color represents the localization of electrons that are low. From Fig. 9, the red and blue colors in the LOL graph correspond to the values between 0.000 and 0.800, within the range of −15.67 to 15.67, −9.89 to 19.78, −18.60 to 9.30, and −9.63 to 19.25 $Bohr^3$ for the TPOXX and TPOXX + Ag/Au/Pt···SiO_2 molecules respectively and the blue-colored region shows the valence shell and inner shell with an electron depletion zone between them and a green colored region indicates strong covalent bonds [47,48].

Table 6
Mulliken atomic charges of TPOXX and TPOXX + Ag/Au/Pt···SiO_2 at gas and water phase calculated by using B3LYP/LANL2DZ basis set.

Atom	TPOXX		TPOXX + Ag···SiO_2		TPOXX + Au···SiO_2		TPOXX + Pt···SiO_2	
	Gas	Water	Gas	Water	Gas	Water	Gas	Water
1F	−0.1930	−0.1989	−0.1954	−0.2003	−0.1889	−0.2005	−0.1905	−0.1973
2F	−0.1914	−0.1984	−0.1932	−0.1992	−0.1909	−0.1981	−0.1876	−0.1961
3F	−0.1918	−0.2021	−0.1936	−0.2032	−0.1912	−0.1978	−0.1888	−0.2000
4O	−0.2138	−0.2630	−0.2637	−0.2856	−0.2093	−0.2612	−0.1841	−0.2466
5O	−0.2119	−0.2614	−0.2015	−0.2466	−0.2124	−0.2598	−0.2115	−0.2569
6O	−0.2613	−0.3093	−0.2428	−0.2956	−0.2626	−0.2905	−0.3598	−0.3832
7 N	−0.1603	−0.1577	−0.1550	−0.1536	−0.1695	−0.1676	−0.1921	−0.1912
8 N	−0.3764	−0.3824	−0.3782	−0.3786	−0.3646	−0.3690	−0.3507	−0.3555
9C	−0.2238	−0.2283	−0.2252	−0.2289	−0.2233	−0.2281	−0.2291	−0.2333
10C	−0.2242	−0.2288	−0.2242	−0.2277	−0.2233	−0.2263	−0.2246	−0.2271
11C	−0.5091	−0.5282	−0.5078	−0.5282	−0.5072	−0.5288	−0.5100	−0.5320
12C	−0.1679	−0.1708	−0.1714	−0.1715	−0.1826	−0.1857	−0.1899	−0.1964
13C	−0.1681	−0.1711	−0.1680	−0.1715	−0.1783	−0.1824	−0.1723	−0.1779
14C	−0.2102	−0.2180	−0.2158	−0.2206	−0.2086	−0.2161	−0.1857	−0.1972
15C	−0.2073	−0.2148	−0.2107	−0.2173	−0.2049	−0.2122	−0.2041	−0.2103
16C	−0.2367	−0.2572	−0.2227	−0.2423	−0.2045	−0.2170	−0.2321	−0.2274
17C	−0.2385	−0.2582	−0.2502	−0.2654	−0.2349	−0.2509	−0.2535	−0.2704
18C	0.1628	0.1828	0.2656	0.2747	0.1739	0.1963	0.1696	0.2099
19C	0.1625	0.1814	0.1542	0.1775	0.1620	0.1841	0.1685	0.1970
20C	0.2245	0.2146	0.2125	0.2190	0.2828	0.2680	0.3483	0.3405
21C	0.3329	0.3423	0.3429	0.3479	0.3317	0.3389	0.3153	0.3272
22C	−0.3429	−0.3554	−0.3613	−0.3831	−0.3086	−0.3198	−0.3132	−0.3232
23C	−0.3541	−0.3493	−0.3772	−0.3648	−0.3608	−0.3538	−0.3492	−0.3411
24C	−0.3292	−0.3356	−0.3497	−0.3549	−0.3379	−0.3421	−0.3312	−0.3376
25C	−0.3413	−0.3453	−0.3431	−0.3455	−0.3411	−0.3462	−0.3411	−0.3451
26C	0.3359	0.3371	0.3319	0.3301	0.3380	0.3399	0.3360	0.3387
27C	0.3192	0.3200	0.3139	0.3148	0.3177	0.3180	0.3211	0.3206
28H	0.2376	0.2560	0.2413	0.2581	0.2387	0.2570	0.2404	0.2577
29H	0.2377	0.2561	0.2408	0.2581	0.2380	0.2570	0.2399	0.2583
30H	0.2353	0.2331	0.2375	0.2341	0.2397	0.2335	0.2394	0.2334
31H	0.2264	0.2374	0.2302	0.2391	0.2277	0.2382	0.2275	0.2372
32H	0.2451	0.2502	0.2539	0.2567	0.2506	0.2526	0.2512	0.2511
33H	0.2454	0.2503	0.2479	0.2531	0.2451	0.2506	0.2425	0.2480
34H	0.2586	0.2917	0.2706	0.3022	0.2600	0.2931	0.2586	0.2903
35H	0.2588	0.2919	0.2657	0.2984	0.2600	0.2934	0.2589	0.2927
36H	0.2390	0.2484	0.2467	0.2473	0.2522	0.2494	0.3291	0.3105
37H	0.2396	0.2488	0.2444	0.2530	0.2406	0.2481	0.2444	0.2487
38H	0.3383	0.3809	0.3523	0.3892	0.3464	0.3888	0.3484	0.3922
39H	0.2762	0.2811	0.3619	0.3516	0.2683	0.2745	0.2804	0.2804
40H	0.2498	0.2724	0.2639	0.2793	0.2574	0.2767	0.2557	0.2758
41H	0.2640	0.2785	0.2639	0.2738	0.2642	0.2793	0.2701	0.2815
42H	0.2635	0.2794	0.2619	0.2787	0.2660	0.2806	0.2677	0.2819
43Si			0.6932	0.6393	0.9324	0.9047	0.9545	0.8859
44O			−0.8259	−0.8883	−0.8267	−0.9026	−0.8603	−0.8760
45O			−0.8711	−0.8977	−0.8369	−0.8842	−0.8158	−0.8663
46Si			0.6805	0.6395	0.9312	0.9055	0.9528	0.8504
47Ag			−0.2643	−0.2311				
48Ag			0.4346	0.5861				
47Au					−0.7006	−0.7019		
48Au					0.3448	0.5144		
47 Pt							−0.2661	−0.2411
48 Pt							−0.1768	0.0193

Table 7
Computed thermodynamic properties of TPOXX and TPOXX + Ag/Au/Pt···SiO_2 at gas and water by using B3LYP/LANL2DZ basis set.

	TPOXX		TPOXX + Ag–SiO_2		TPOXX + Au–SiO_2		TPOXX + Pt–SiO_2	
	Gas	Water	Gas	Water	Gas	water	Gas	water
Enthalpy ΔH (Hartree)	−1367.2	−1367.3	−1817	−1817	−1796.4	−1796.4	−1763.8	−1763.8
Gibbs free energy ΔG (Hartree)	−1367.3	−1367.3	−1817.1	−1817.2	−1796.5	−1796.5	−1763.9	−1763.9
Energy ΔE (KCal/Mol)	211.3	209.8	223.7	222.1	223.9	222.4	224.3	222.2
Specific heat capacityCv (Cal/mol-Kelvin)	85.1	81.4	115.8	112.2	115.4	111.9	114.6	108.9
Entropy(Cal/mol-Kelvin)	162.3	152.3	218.0	208.3	228.3	216.2	216.8	198.5

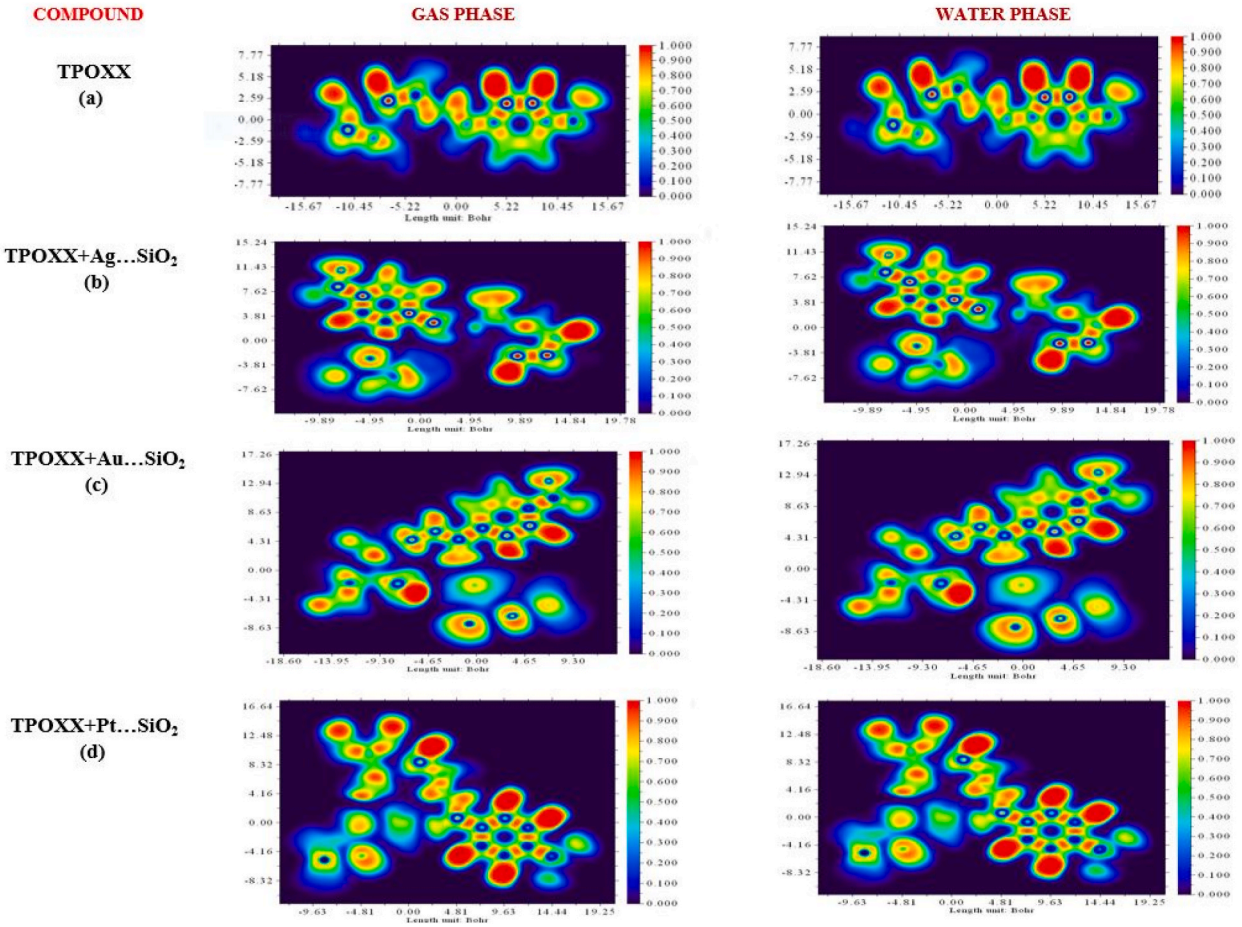

Fig. 7. ELF color filled plots of (a) TPOXX, (b) TPOXX + Ag···SiO_2,(c) TPOXX + Au···SiO_2, (d) TPOXX + Pt···SiO_2 at gas and water phase. (For interpretation of the references to color in this figure legend, the reader is referred to the Web version of this article.)

3.9. Drug-likeness and lipophilicity properties analysis

Drug-likeness refers to the set of physicochemical and structural properties that a molecule must possess to have the potential to become a drug by measuring the bioavailability of the molecule [49–51]. Some of the factors that are commonly considered when evaluating the drug-likeness of a molecule include its molecular weight, lipophilicity, hydrogen bond donors, hydrogen bond acceptors, TPSA, solubility, and bioavailability scores. These scores were predicted using the Swiss ADME tool, and the values are tabulated in Table 8(a). As per Lipinski's rule, a compound will have good oral bioavailability if it meets the following criteria: The MW should be $\leq$ 500 g/mol; $\leq$ 5H bond donors and $\leq$10 H bond acceptors; the TPSA should be $\leq$ 140 Å; and the molar reactivity should be 40–130. If the molecules violate more than one of these rules, they are more likely to have poor absorption, making them less effective as drugs. From the observation, the title molecule and the complexes (Ag/Au/Pt···SiO_2) show an excellent bioactivity score. So that they can be used as a candidate for a drug. The lipophilicity properties such as XLOGP3, WLOGP, MLOGP, SILICOS-IT-LOGP, and ilogp [52] were listed in Table 8(b), and they refer to the ability of the molecule to dissolve in the human lipid system.

3.10. Molecular docking analysis

Molecular docking is used to forecast the mechanism and affinities of a ligand's binding to a target protein or receptor. Virtual screening can be performed with the aid of iGEMDOCK software. In addition to molecular docking, it can be used sequentially to prepare targets, databases, dock molecules, and analyze their conformations. The first step was to specify target protein atom coordinates from the PDB, the ligand binding area, atom formal charge, and atom type. As a second capability, it may be used to sequentially read the coordinates of an atom in the ligand from a prepared database of ligands. Following the preparation of the ligand database and the target protein, it performs flexible docking for each ligand sequentially. The final step in iGEMDOCK's post-docking analysis is to rank and sort all docked ligand conformations. Empirical and evolutionary scoring functions are used in this dock. Potentials for electrostatic, steric, and hydrogen bonds are included in iGEMDOCK's energy function. As a result of these two terms, a

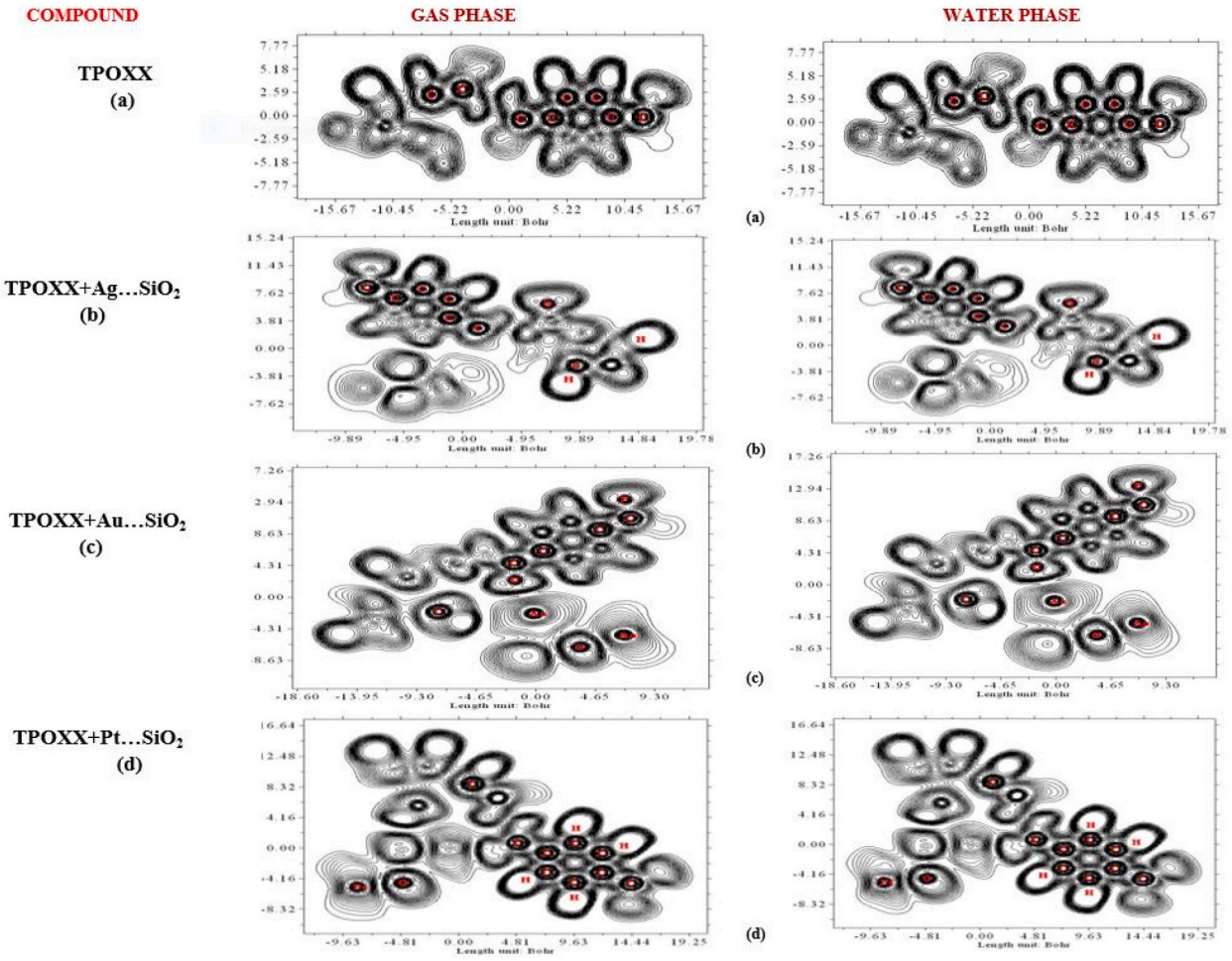

Fig. 8. ELF contour plots of (a) TPOXX, (b) TPOXX + Ag···SiO_2, (c) TPOXX + Au···SiO_2 (d) TPOXX + Pt···SiO_2 at gas and water phase.

linear model is employed that is simple and rapidly recognizes potential complexes. Multi-operator cooperative approaches use a family competition paradigm, which is similar to a local search process, to implement this evolutionary approach.

The Protein Data Bank (PDB ID: 5R7Y, 6M0J, and 6WRH) was used to obtain the crystal structures of the COVID-19 main protease at 1.65 Å resolution, the SARS-CoV-2 spike protein bound to angiotensin converting enzyme 2 (ACE2) at 2.45 Å resolution, and the SARS-CoV-2 papin like protease mutant C111S at 1.60 Å resolution [53]. The crystal structure of TPOXX drug molecule and TPOXX + Ag/Au/Pt···SiO_2 complexes possessing hydrogen bond energy and van der Waals energy are tabulated in Table 9. The TPOXX and TPOXX + Ag/Au/Pt···SiO_2 interacts very well with the inhibitor, and the results are revealed in Fig. 11. The docking energy of TPOXX is higher at −96.245 with the S-protein (6M0J). For the complexes TPOXX + Ag/Au/Pt···SiO_2, the highest docking energy (−106.748), is found at TPOXX + Au···SiO_2 with the same S-protein 6MOJ and the least docking energy is found at TPOXX + Pt···SiO_2 with M^{pro} protein 5R7Y. TPOXX + Ag/Au/Pt···SiO_2 possesses more van der Waals energy as well as hydrogen energy when compared to the pure TPOXX drug molecule.

4. Conclusion

The adsorption properties of TPOXX over Ag/Au/Pt···SiO_2 silica nanocomposites were investigated theoretically using different computational methods. The adsorption of TPOXX over the silica nanocomposites was investigated with the help of SERS spectra. TPOXX molecule interacts with the silica nanocomposites (Ag/Au/Pt···SiO_2) with adsorption energies of −0.08, −0.41, and −1.63 kcal/mol, respectively, which confirms the bond formation between the TPOXX and silica nanocomposites. The UV–Vis studies have been carried out in which the TPOXX + Ag/Au/Pt...SiO_2 shows the red shift in the UV absorption. The thermodynamic properties of TPOXX and TPOXX + Ag/Au/Pt...SiO2 are examined for different terms of Gibbs free energy (ΔG), entropy, and enthalpy (ΔH). TPOXX and TPOXX + Ag/Au/Pt...SiO_2 molecules were subjected to druglikeness and lipophilicity properties, which show that all complexes obey the Lipinski rule. The ELF and LOL topological analysis were also carried out. To check the anti-covid activity of the molecule, the anti-viral drug TPOXX and its silica nanocomposites complexes were docked with the different crystal structures of SARS-CoV-2

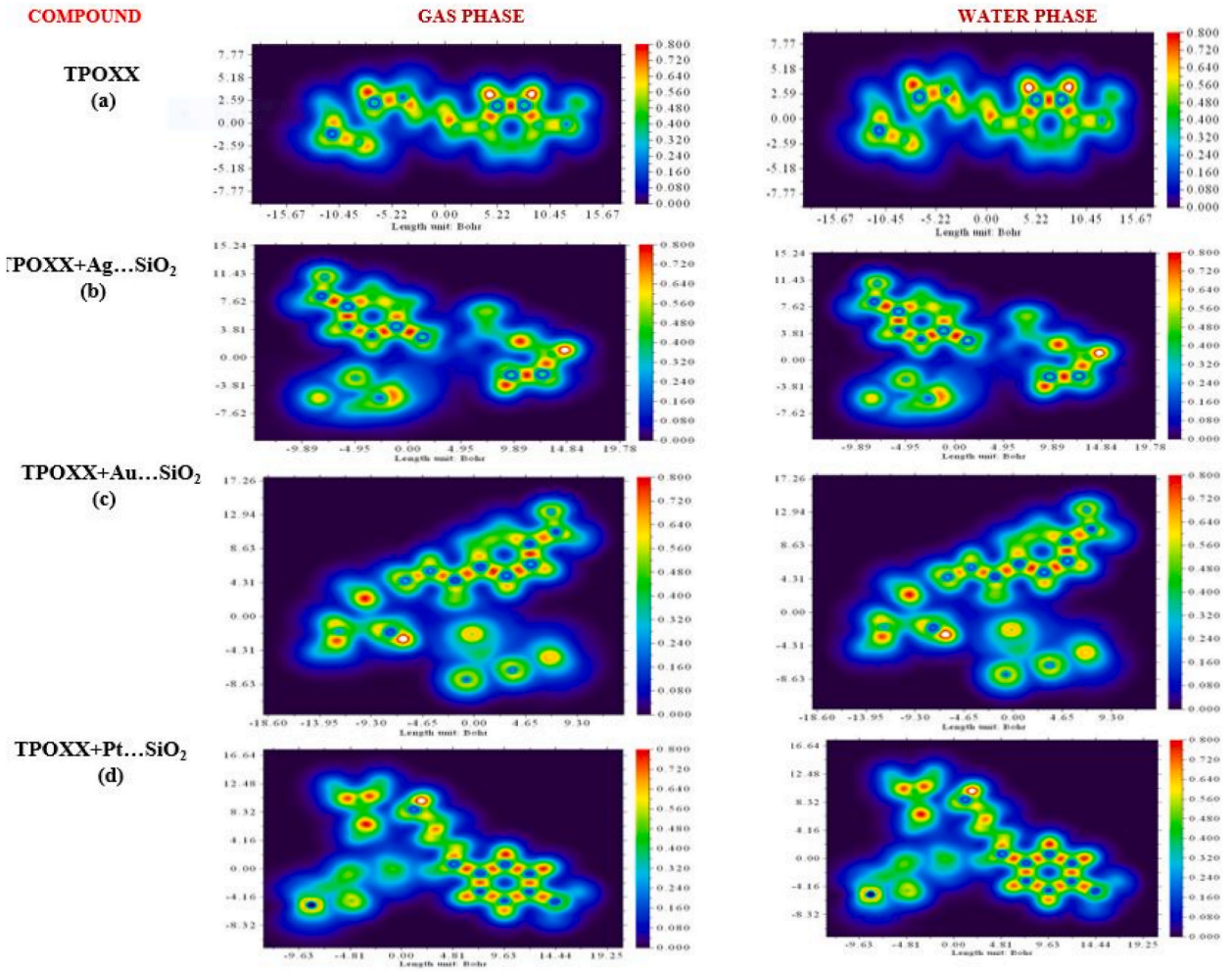

Fig. 9. LOL color filled plots of (a) TPOXX, (b) TPOXX + Ag···SiO_2, (c) TPOXX + Au···SiO_2,(d) TPOXX + Pt···SiO_2 at gas and water phase. (For interpretation of the references to color in this figure legend, the reader is referred to the Web version of this article.)

receptors. The complexes TPOXX + Ag/Au/Pt···SiO_2 possess more van der Waals energy and hydrogen energy compared to the title molecule, and it endorses that the TPOXX along with the silica nanocomposites (Ag/Au/Pt···SiO_2) exhibit inhibitory properties and may prevent the development of anti-viral and anti-covid properties.

Data availability statement

Data will be made available on request.

Funding statement

This research did not receive any specific grant from funding agencies in the public, commercial, or not-for-profit sectors.

CRediT authorship contribution statement

Nivetha G F: Conceptualization, Data curation, Formal analysis, Investigation, Methodology, Validation, Writing – original draft, Writing – review & editing. **Vetrivelan V:** Conceptualization, Investigation, Methodology, Resources, Software, Writing – original draft, Writing – review & editing. **Govindammal M:** Formal analysis, Investigation, Methodology. **Muthu S:** Formal analysis, Resources, Software. **Prasath M:** Conceptualization, Formal analysis, Project administration, Supervision, Validation, Writing – original draft, Writing – review & editing.

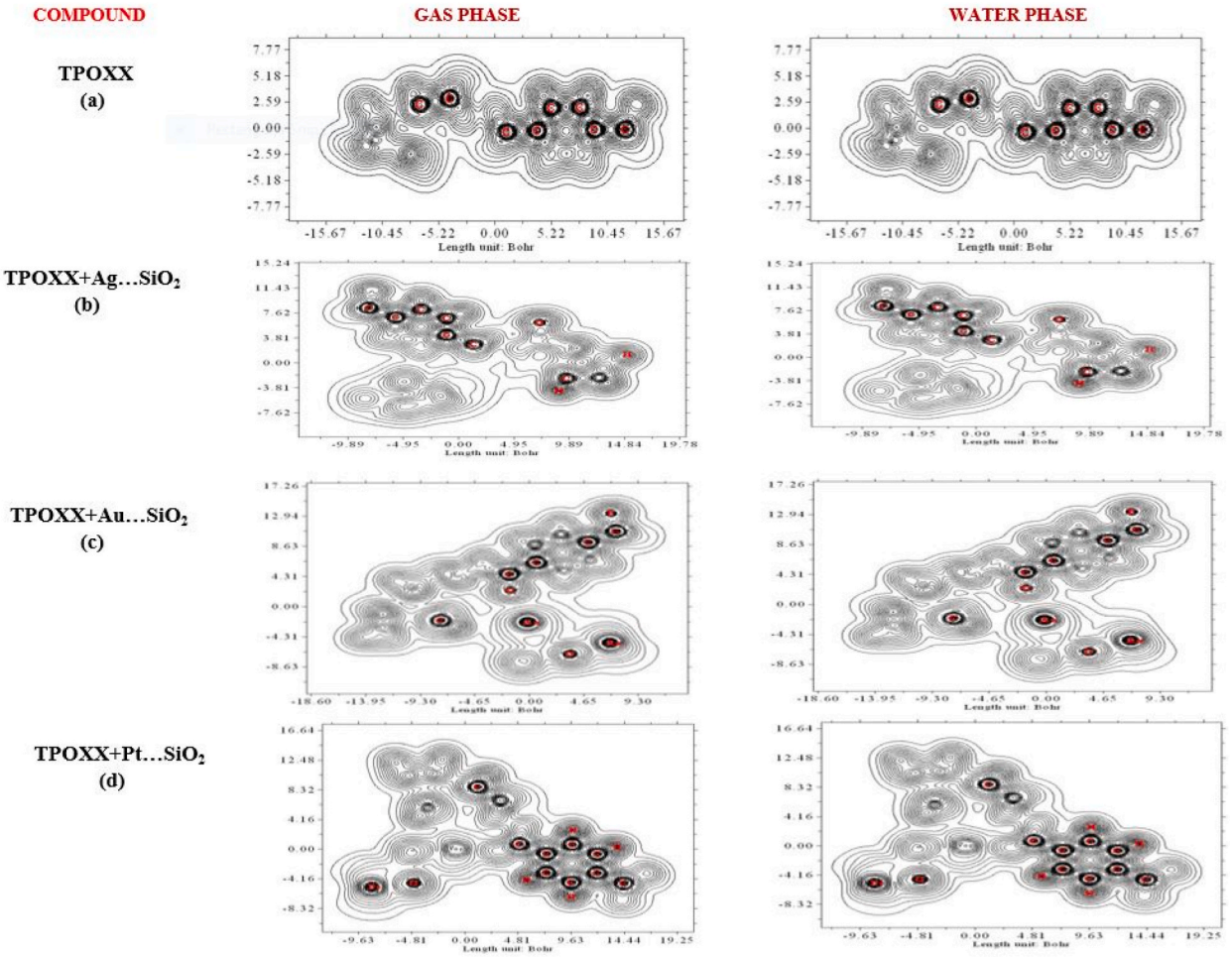

Fig. 10. LOL contour plots of (a) TPOXX, (b) TPOXX + Ag···SiO_2,(c) TPOXX + Au···SiO_2 (d) TPOXX + Pt···SiO_2 at gas and water phase.

Table 8a
Druglikeness parameters of TPOXX and TPOXX + Ag/Au/Pt···SiO_2.

	TPOXX	TPOXX + Ag···SiO_2	TPOXX + Au···SiO_2	TPOXX + Pt···SiO_2
Rotatable bonds	4	4	4	4
Hydrogen bond acceptors	6	8	8	8
Hydrogen bond donors	1	1	1	1
Molar refractivity	90.79	104.47	104.47	104.47
Topological polar surface area	66.48	91.54	91.54	91.54
Bioavailability score	0.55	0.55	0.55	0.55
Pure water solubility	7.2	1.6	1.58	1.66
Log kp	−6.74	−8.53	−9.62	−9.6
Lipinski rule violations	0	1	1	1

Table 8b
Lipophilicity parameters of TPOXX and TPOXX + Ag/Au/Pt···SiO_2.

	TPOXX	TPOXX + Ag···SiO_2	TPOXX + Au···SiO_2	TPOXX + Pt···SiO_2
ilogP	2.13	0	0	0
XLOGP3	2.61	2.7	2.7	2.7
WLOGP	3.17	2.28	2.27	2.27
MLOGP	3.5	1.89	1.89	1.89
Silicos-IT LogP	1.82	1.82	1.82	1.82
Consenus Log P	2.65	1.74	1.74	1.74

Table 9
Binding energies between ligands (TPOXX and TPOXX + Ag/Au/Pt···SiO_2) and proteins obtained from docking studies.

Ligand	Protein	Total energy	VDW	H-Bond
TPOXX	5R7Y	−86.1805	−71.3113	−14.8692
	6M0J	−96.245	−84.6737	−11.5713
	6WRH	−90.2901	−76.7909	−13.4992
TPOXX + Ag···SiO_2	5R7Y	−100.112	−76.7125	−23.3991
	6M0J	−104.792	−89.325	−15.4666
	6WRH	−104.719	−84.993	−19.7261
TPOXX + Au···SiO_2	5R7Y	−90.3796	−86.3031	−4.07649
	6M0J	−106.748	−98.0601	−8.68773
	6WRH	−94.0403	−80.886	−13.1543
TPOXX + Pt···SiO_2	5R7Y	−87.4074	−72.1755	−15.2319
	6M0J	−97.8632	−91.6962	−6.16699
	6WRH	−90.6783	−76.4477	−14.2305

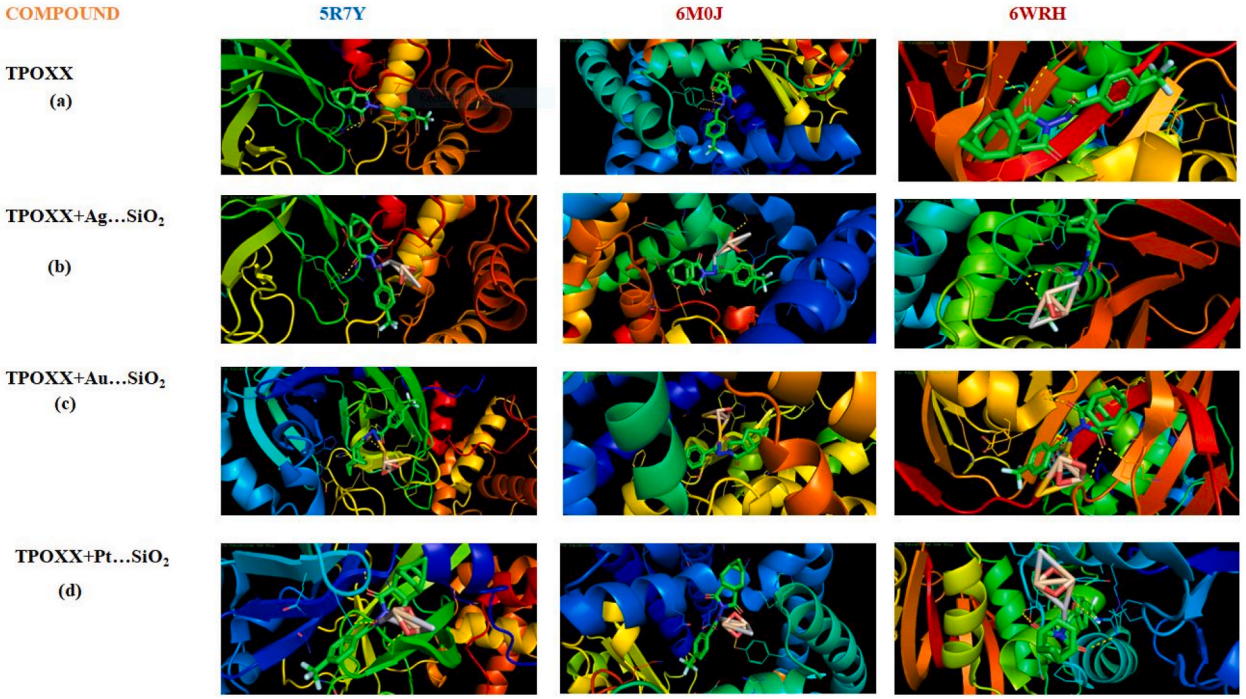

Fig. 11. Interactions of ligands (a) TPOXX, (b) TPOXX + Ag···SiO_2, (c) TPOXX + Au···SiO_2, (d) TPOXX + Pt···SiO_2 with targeted proteins.

Declaration of competing interest

The authors declare that they have no known competing financial interests or personal relationships that could have appeared to influence the work reported in this paper.

References

[1] N. Shaghaghi, Molecular docking study of novel COVID-19 protease with low risk terpenoides compounds of plants, Chem 1 (2020), https://doi.org/10.26434/chemrxiv.11935722.v1.
[2] WHO Coronavirus (COVID-19) Dashboard, World Health Organization, 2023. https://covid19.who.int/.
[3] W.R. Matias, J.M. Koshy, E.H. Nagami, V. Kovac, L.R. Moeng, E.S. Shenoy, D.C. Hooper, L.C. Madoff, M.B. Barshak, J.A. Johnson, C.F. Rowley, B. Julg, E. L. Hohmann, J.E. Lazarus, Tecovirimat for the treatment of human monkeypox: an initial series from Massachusetts, United States, open forum infect, Dissent 9 (2022), https://doi.org/10.1093/ofid/ofac377 ofac377.
[4] K. Sarkar, R.K. Das, Repurposing of existing pharmaceutical drugs against monkey-pox virus: an in silico study, Anal. Chem. Lett. 12 (2022) 655–670, https://doi.org/10.1080/22297928.2022.2157224.
[5] F. Mollaamin, S. Shahriari, M. Monajjemi, Monkeypox disease treatment by tecovirimat adsorbed onto single-walled carbon nanotube through drug delivery method, J. Chil. Chem. Soc. 68 (2023) 5796–5801, https://doi.org/10.4067/S0717-97072023000105796.
[6] G. Yang, D.C. Pevear, M.H. Davies, M.S. Collett, T. Bailey, S. Rippen, L. Barone, C. Burns, G. Rhodes, S. Tohan, J.W. Huggins, R.O. Baker, R.L.M. Buller, E. Touchette, K. Waller, J. Schriewer, J. Neyts, E. DeClercq, K. Jones, D. Hruby, R. Jordan, An orally bioavailable antipoxvirus compound (ST-246) inhibits

extracellular virus formation and protects mice from lethal orthopoxvirus Challenge, J. Virol. 79 (2005) 13139–13149, https://doi.org/10.1128/JVI.79.20.13139-13149.2005.
[7] Y. Chen, K.M. Honeychurch, G. Yang, C.M. Byrd, C. Harver, D.E. Hruby, R. Jordan, Vaccinia virus p37 interacts with host proteins associated with LE-derived transport vesicle biogenesis, Virol. J. 6 (2009) 44, https://doi.org/10.1186/1743-422X-6-44.
[8] R. Blasco, B. Moss, Extracellular vaccinia virus formation and cell-to-cell virus transmission are prevented by deletion of the gene encoding the 37,000-Dalton outer envelope protein, J. Virol. 65 (1991) 5910–5920, https://doi.org/10.1128/JVI.65.11.5910-5920.1991.
[9] L.G. Payne, Significance of extracellular enveloped virus in the in vitro and in vivo dissemination of vaccinia, J. Gen. Virol. 50 (1980) 89–100, https://doi.org/10.1099/0022-1317-50-1-89.
[10] I. Gurt, I. Abdalrhman, E. Katz, Pathogenicity and immunogenicity in mice of vaccinia viruses mutated in the viral envelope proteins A33R and B5R, Antivir. Res. 69 (2006) 158–164, https://doi.org/10.1016/j.antiviral.2005.11.006.
[11] A.A. McIntosh, G.L. Smith, Vaccinia virus glycoprotein A34R is required for infectivity of extracellular enveloped virus, J. Virol. 70 (1996) 272–281, https://doi.org/10.1128/JVI.70.1.272-281.1996.
[12] E.J. Wolffe, S.N. Isaacs, B. Moss, Deletion of the vaccinia virus B5R gene encoding a 42-kilodalton membrane glycoprotein inhibits extracellular virus envelope formation and dissemination, J. Virol. 67 (1993) 4732–4741, https://doi.org/10.1128/JVI.67.8.4732-4741.1993.
[13] S.M. Hoy, Tecovirimat: first global approval, Drugs 78 (2018) 1377–1382, https://doi.org/10.1007/s40265-018-0967-6.
[14] S.D. Brown, P. Nativo, J.-A. Smith, D. Stirling, P.R. Edwards, B. Venugopal, D.J. Flint, J.A. Plumb, D. Graham, N.J. Wheate, Gold nanoparticles for the improved anticancer drug delivery of the active component of oxaliplatin, J. Am. Chem. Soc. 132 (2010) 4678–4684, https://doi.org/10.1021/ja908117a.
[15] N. Chanda, V. Kattumuri, R. Shukla, A. Zambre, K. Katti, A. Upendran, R.R. Kulkarni, P. Kan, G.M. Fent, S.W. Casteel, C.J. Smith, E. Boote, J.D. Robertson, C. Cutler, J.R. Lever, K. V Katti, R. Kannan, Bombesin functionalized gold nanoparticles show in vitro and in vivo cancer receptor specificity, Proc. Natl. Acad. Sci. USA 107 (2010) 8760–8765, https://doi.org/10.1073/pnas.1002143107.
[16] V. Chandrakala, V. Aruna, G. Angajala, Review on metal nanoparticles as nanocarriers: current challenges and perspectives in drug delivery systems, Emergent Mater 5 (2022) 1593–1615, https://doi.org/10.1007/s42247-021-00335-x.
[17] N. Mahar, V. Vetrivelan, S. Muthu, S. Javed, A.A. Al-Saadi, Surface enhanced Raman spectra (SERS) and computational study of gemcitabine drug adsorption on to Au/Ag clusters with different complexes: adsorption behavior and solvent effect (IEFPCM) – anticancer agent, Comput. Theor. Chem. 1217 (2022), 113914, https://doi.org/10.1016/j.comptc.2022.113914.
[18] V. Vetrivelan, S. Sakthivel, S. Muthu, A.A. Al-Saadi, Non-covalent interaction, adsorption characteristics and solvent effect of procainamide anti-arrhythmias drug on silver and gold loaded silica surfaces: SERS spectroscopy, density functional theory and molecular docking investigations, RSC Adv. 13 (2023) 9539–9554, https://doi.org/10.1039/D3RA00514C.
[19] Y. Wang, Q. Zhao, N. Han, L. Bai, J. Li, J. Liu, E. Che, L. Hu, Q. Zhang, T. Jiang, S. Wang, Mesoporous silica nanoparticles in drug delivery and biomedical applications, Nanomed. Nanotechnol. Biol. Med. 11 (2015) 313–327, https://doi.org/10.1016/j.nano.2014.09.014.
[20] M. Younes, P. Aggett, F. Aguilar, R. Crebelli, B. Dusemund, M. Filipič, M.J. Frutos, P. Galtier, D. Gott, U. Gundert-Remy, G.G. Kuhnle, J.-C. Leblanc, I. T. Lillegaard, P. Moldeus, A. Mortensen, A. Oskarsson, I. Stankovic, I. Waalkens-Berendsen, R.A. Woutersen, M. Wright, P. Boon, D. Chrysafidis, R. Gürtler, P. Mosesso, D. Parent-Massin, P. Tobback, N. Kovalkovicova, A.M. Rincon, A. Tard, C. Lambré, Re-evaluation of silicon dioxide (E 551) as a food additive, EFSA J. 16 (2018), e05088, https://doi.org/10.2903/j.efsa.2018.5088.
[21] M. Vallet-Regí, F. Balas, Silica materials for medical applications, Open Biomed. Eng. J. 2 (2008) 1–9, https://doi.org/10.2174/1874120700802010001.
[22] J. Alimunnisa, K. Ravichandran, K.S. Meena, Synthesis and characterization of Ag@SiO_2 core-shell nanoparticles for antibacterial and environmental applications, J. Mol. Liq. 231 (2017) 281–287, https://doi.org/10.1016/j.molliq.2017.01.103.
[23] N. Subbiah, T. Palanisamy, Collagen-supported amino-functionalized Ag@SiO_2 core–shell nanoparticles for visible-light-driven water remediation, ACS Appl. Nano Mater. 5 (2022) 14408–14424, https://doi.org/10.1021/acsanm.2c02751.
[24] P.A. Mosier-Boss, Review of SERS substrates for chemical sensing, Nanomaterials 7 (2017), https://doi.org/10.3390/nano7060142.
[25] B. Sharma, R.R. Frontiera, A.-I. Henry, E. Ringe, R.P. Van Duyne, SERS: materials, applications, and the future, Mater. Today 15 (2012) 16–25, https://doi.org/10.1016/S1369-7021(12)70017-2.
[26] J. Osipiuk, S.-A. Azizi, S. Dvorkin, M. Endres, R. Jedrzejczak, K.A. Jones, S. Kang, R.S. Kathayat, Y. Kim, V.G. Lisnyak, S.L. Maki, V. Nicolaescu, C.A. Taylor, C. Tesar, Y.-A. Zhang, Z. Zhou, G. Randall, K. Michalska, S.A. Snyder, B.C. Dickinson, A. Joachimiak, Structure of papain-like protease from SARS-CoV-2 and its complexes with non-covalent inhibitors, Nat. Commun. 12 (2021) 743, https://doi.org/10.1038/s41467-021-21060-3.
[27] S. Chtita, S. Belaidi, F.A. Qais, M. Ouassaf, M.M. AlMogren, A.A. Al-Zahrani, M. Bakhouch, A. Belhassan, H. Zaki, M. Bouachrine, T. Lakhlifi, Unsymmetrical aromatic disulfides as SARS-CoV-2 Mpro inhibitors: molecular docking, molecular dynamics, and ADME scoring investigations, J. King Saud Univ. Sci. 34 (2022), 102226, https://doi.org/10.1016/j.jksus.2022.102226.
[28] S. Chtita, R.T. Fouedjou, S. Belaidi, L.A. Djoumbissie, M. Ouassaf, F.A. Qais, M. Bakhouch, M. Efendi, T.T. Tok, M. Bouachrine, T. Lakhlifi, In silico investigation of phytoconstituents from Cameroonian medicinal plants towards COVID-19 treatment, Struct. Chem. 33 (2022) 1799–1813, https://doi.org/10.1007/s11224-022-01939-7.
[29] I. Yamari, O. Abchir, S.N. Mali, A. Errougui, M. Talbi, M. El Kouali, S. Chtita, The anti-SARS-CoV-2 activity of novel 9, 10-dihydrophenanthrene derivatives: an insight into molecular docking, ADMET analysis, and molecular dynamics simulation, Sci. African. 21 (2023), e01754, https://doi.org/10.1016/j.sciaf.2023.e01754.
[30] A. Belhassan, H. Zaki, S. Chtita, M. Alaqarbeh, N. Alsakhen, M. Benlyas, T. Lakhlifi, M. Bouachrine, Camphor, artemisinin and sumac phytochemicals as inhibitors against COVID-19: computational approach, Comput. Biol. Med. 136 (2021), 104758, https://doi.org/10.1016/j.compbiomed.2021.104758.
[31] A. Belhassan, S. Chtita, H. Zaki, M. Alaqarbeh, N. Alsakhen, F. Almohtaseb, T. Lakhlifi, M. Bouachrine, In silico detection of potential inhibitors from vitamins and their derivatives compounds against SARS-CoV-2 main protease by using molecular docking, molecular dynamic simulation and ADMET profiling, J. Mol. Struct. 1258 (2022), 132652, https://doi.org/10.1016/j.molstruc.2022.132652.
[32] Y. Huang, C. Yang, X. Xu, W. Xu, S. Liu, Structural and functional properties of SARS-CoV-2 spike protein: potential antivirus drug development for COVID-19, Acta Pharmacol. Sin. 41 (2020) 1141–1149, https://doi.org/10.1038/s41401-020-0485-4.
[33] M.J. Frisch, G.W. Trucks, H.B. Schlegel, G.E. Scuseria, M.A. Robb, J.R. Cheeseman, G. Scalmani, V. Barone, B. Mennucci, G.A. Petersson, H. Nakatsuji, M. Caricato, X. Li, H.P. Hratchian, A.F. Izmaylov, J. Bloino, G. Zheng, J.L. Sonnenberg, M. Had, W. C, Complete List of Authors of Gaussian, 9, 2014, pp. 1–6.
[34] E. Frisch, H.P. Hratchian, R.D. Dennington II, et al., Gaussview, 8, Gaussian Inc., Wallingford, CT, 2009, p. 235, Version 5.0.
[35] T. Lu, F. Chen, Multiwfn: a multifunctional wavefunction analyzer, J. Comput. Chem. 33 (2012) 580–592, https://doi.org/10.1002/jcc.22885.
[36] Swiss ADME, http://www.swissadme.ch/.
[37] Passonline, http://www.way2drug.com/passonline/.
[38] Protein Data Bank PDB, https://www.rcsb.org/.
[39] K.-C. Hsu, Y.-F. Chen, S.-R. Lin, J.-M. Yang, iGEMDOCK: a graphical environment of enhancing GEMDOCK using pharmacological interactions and post-screening analysis, BMC Bioinf. 12 (2011) S33, https://doi.org/10.1186/1471-2105-12-S1-S33.
[40] J.S. Al-Otaibi, Y.S. Mary, Y.S. Mary, Z. Ullah, R. Yadav, N. Gupta, D.G. Churchill, Adsorption properties of dacarbazine with graphene/fullerene/metal nanocages – reactivity, spectroscopic and SERS analysis, Spectrochim. Acta Part A Mol. Biomol. Spectrosc. 268 (2022), 120677, https://doi.org/10.1016/j.saa.2021.120677.
[41] The PyMOL Molecular Graphics System, Version 4.6 Schrodinger, LLC.
[42] J.S. Al-Otaibi, P. Albrycht, Y.S. Mary, Y.S. Mary, M. Księżopolska-Gocalska, Concentration-dependent SERS profile of olanzapine on silver and silver-gold metallic substrates, Chem. Pap. 75 (2021) 6059–6072, https://doi.org/10.1007/s11696-021-01783-9.
[43] N. Mani, B. Sathya, M. Prasath, Spectroscopic, quantum chemical, ADMET and molecular docking studies of echinatin: a prospective tuberculosis drug, Res. Chem. Intermed. 48 (2022) 2363–2390, https://doi.org/10.1007/s11164-022-04716-7.

[44] H. Xu, D.C. Xu, Y. Wang, Natural indices for the chemical hardness/softness of metal cations and ligands, ACS Omega 2 (2017) 7185–7193, https://doi.org/10.1021/acsomega.7b01039.
[45] S. Bangaru, P. Manivannan, Probing the structural properties, binding mode and intermolecular interactions of herbacetin against H1N1 neuraminidase using vibrational spectroscopic, quantum chemical calculation and molecular docking studies, Res. Chem. Intermed. 47 (2021) 2775–2799, https://doi.org/10.1007/s11164-021-04408-8.
[46] J.S. Al-Otaibi, Y.S. Mary, Y.S. Mary, DFT analysis of valproic acid adsorption onto Al12/B12-N12/P12 nanocages with solvent effects, J. Mol. Model. 28 (2022) 98, https://doi.org/10.1007/s00894-022-05088-w.
[47] S. Chithra, G. Mani, M. Kumar, V. Vetrivelan, S. Muthu, K. Arulaabaranam, A. Jeelani, A. Irfan, H. Umamahesvari, Theoretical electron excitation study in liquid phase (protic, aprotic, non-polar) and inter and intra molecular reactivity of 2-hydroxy-5-[1-hydroxy-2-(4-phenylbutan-2-ylamino) ethyl] benzamide, J. Indian Chem. Soc. 99 (2022), 100372, https://doi.org/10.1016/j.jics.2022.100372.
[48] B. Silvi, A. Savin, Classification of chemical bonds based on topological analysis of electron localization functions, Nature 371 (1994) 683–686, https://doi.org/10.1038/371683a0.
[49] M. Govindammal, S. Kannan, P. Srinivasan, M. Prasath, Quantum chemical calculations, spectroscopic studies and molecular docking investigations of the anti-cancer drug quercitrin with B-RAF inhibitor, Heliyon 8 (2022), e09539, https://doi.org/10.1016/j.heliyon.2022.e09539.
[50] M. Chalkha, M. Akhazzane, F.Z. Moussaid, O. Daoui, A. Nakkabi, M. Bakhouch, S. Chtita, S. Elkhattabi, A.I. Housseini, M. El Yazidi, Design, synthesis, characterization, in vitro screening, molecular docking, 3D-QSAR, and ADME-Tox investigations of novel pyrazole derivatives as antimicrobial agents, New J. Chem. 46 (2022) 2747–2760, https://doi.org/10.1039/D1NJ05621B.
[51] M. Ouassaf, S. Belaidi, S. Khamouli, H. Belaidi, S. Chtita, Combined 3D-QSAR and molecular docking analysis of thienopyrimidine derivatives as Staphylococcus aureus inhibitors, Acta Chim. Slov. 68 (2021) 289–303, https://doi.org/10.17344/acsi.2020.5985.
[52] I. Moriguchi, S. Hirono, I. Nakagome, H. Hirano, Comparison of reliability of log P values for drugs calculated by several methods, Chem. Pharm. Bull. (Tokyo) 42 (1994) 976–978, https://doi.org/10.1248/cpb.42.976.
[53] G.F. Nivetha, V. Vetrivelan, S. Muthu, M. Prasath, Adsorption behavior, different green solvent effect and surface enhanced Raman spectra (SERS) investigation on inhibition of SARS-CoV-2 by antineoplastic drug Carmofur with silver/gold/platinum loaded silica nanocomposites: a combined computational analysis and molecular modelling approach, Results Chem 6 (2023), 101096, https://doi.org/10.1016/j.rechem.2023.101096.